



Cite this: *Phys. Chem. Chem. Phys.*,
2019, 21, 12265

Role of the hydrogen bond lifetimes and rotations at the water/amorphous silica interface on proton transport

Jesse Lentz and Stephen H. Garofalini *

Using a highly robust and reactive all-atom potential, molecular dynamics computer simulations have been used to provide detailed analysis of the behavior of water and protons at a large-scale amorphous silica surface that offers the heterogeneity of surface sites and water/silica interactions. Structural data of the H–O distances as a function of distance from the glass surface showed variation in hydrogen bond (H-bond) lengths to second and third nearest oxygen neighbors that play an important role in H-bond lifetimes, rotations, and proton transfer, especially at the glass surface. The higher density and inherently closer average spacing between oxygens in the glass surface (2.6 Å) in comparison to that in water (2.8 Å) create a significantly different environment for H-bond lifetimes and proton transfers. Continuous H-bond lifetime autocorrelation functions for water H-bonded to the surface are considerably shorter than those of bulk water, whereas the intermittent lifetime autocorrelation functions are longer. Such results affect proton transfers that are over an order of magnitude higher at the surface than farther from the surface or in bulk water. However, most of these transfers are rattling events between the participating oxygens, one of which is the newly formed H_3O^+ ion adjacent to the interface. Such a H_3O^+ ion has an extremely low barrier to proton transfer back to the surface site in comparison to a H_3O^+ ion in bulk water. Nonetheless, the simulations showed that rotation of the H_3O^+ ion away from the initial transfer site allowed for structural diffusion of an excess proton away from the surface. Proton conduction from such rotations could be enhanced by external forces.

Received 9th April 2019,
Accepted 21st May 2019

DOI: 10.1039/c9cp01994d

rsc.li/pccp

Introduction

Water at silica surfaces has drawn significant attention due to the reactions that alter the glass surface properties^{1–13} as well as the concomitant effect of the silica surface on the structure and behavior of adjacent water.^{14–27} Additionally, proton mobility on silica surfaces has significant technological relevance; mesoporous silica exhibits anomalously high proton conductivity.^{28–31}

Proton transfer has been well studied in aqueous solutions^{32–40} and the commonly accepted mechanism involves proton transfer *via* a Grotthuss mechanism involving Eigen and Zundel complexes,^{33,39–47} in which extended hydrogen bond (H-bond) arrangements are important.^{48,49} In bulk water, the lifetime of the H_3O^+ ion fluctuates rapidly in the ~ 100 – 200 fs timeframe^{33,50–52} in what are called ‘rattling’ events as the proton transfers from the hydronium ion to the adjacent water molecule in the Zundel complex followed by a rapid return. In the structural diffusion of the H_3O^+ complex, the hydronium ions have lifetimes around 2 ps.⁴²

As shown by Geissler *et al.*, auto-dissociation of the water molecule forming adjacent OH^- and H_3O^+ ions occurs often in bulk water;⁵³ similar behavior was observed in molecular dynamics (MD) simulations of water using the reactive potential employed here.³⁸ However, the simulations also showed that such auto-dissociation is quite short lived in most instances because of the rapid return of the proton to the OH^- ion to reform the neutral waters. Importantly, the lifetimes of H-bonds adjacent to an initial proton exchange event play an important role in the eventual migration of the hydronium complex away from the original event, circumventing rapid neutralization of the product ions. Hence, the behavior of H-bonds on and adjacent to the silica surface are of paramount importance to proton migration at the water/glass interface.

Data obtained from Quasielastic Neutron Scattering (QENS) and nuclear magnetic resonance (NMR) studies of water on crystalline silica (SBA-15) surfaces indicate proton ‘jumps’ but little translational motion of the water molecule.²⁰ In that study, the term ‘jumps’ is meant to convey the rotational distance of the H-bond rotation.²⁰ At low hydration, water molecules can rotate between sites *via* short jumps of 2.5 Å and a characteristic time of 4 ps at 300 K, as well as longer jumps of 4.3 Å at 300 K

Interfacial Molecular Science Laboratory, Department of Materials Science and Engineering, Rutgers University, USA. E-mail: shg@rutgers.edu

and a characteristic time of 25 ps.²⁰ H-bond switches between acceptors with a distance of about 1 Å have been observed in other studies of silica/water interfaces,⁵⁴ but were not conclusively observed by Kiwilsza *et al.*²⁰

Experimental results showing slowed translational motion of water in silica pores have been obtained through NMR and QENS.^{21–24} Simulations have similarly shown slow translational diffusion of water molecules adjacent to the glass surface.⁵⁵ Tsukahara *et al.*, using NMR, showed that rotation and translation of water molecules in nanoporous silica with 40 Å pores are inhibited and proton transfer in larger pores is enhanced by a factor of 10 with respect to bulk water.²⁴ They employ a 3-phase model to describe their findings: an adsorbed water layer, an intermediate layer, and bulk water. Interestingly, they attribute an adsorbed water layer of 3 Å as becoming more important with decreasing pore size. This is consistent with behavior previously observed in simulations that showed the increasingly important role of the 3 Å layer of adsorbed water adjacent to the silica surface (above the GDS) on the increase in the high expansion of nanoconfined water with decreasing pore size.^{25,26}

Also in the Tsukahara *et al.* paper,²⁴ they attribute proton exchange *via* a one-way process from the glass surface to the adsorbed water followed by further exchange to the intermediate water layer, without a reverse process. This may be mechanistically limiting, as shown in our previous MD simulations of proton exchange at silica surfaces that involved proton transfers between water molecules (forming H₃O⁺ ions) and the silica surface sites in both directions due to the variety of sites that are unstable for proton adherence.^{27,56,57} Results similar to the MD simulations of wet silica surfaces have been also observed in DFT studies of silica⁵⁸ and other oxide surfaces.^{59–64} For instance, Merte *et al.* showed significant proton exchange between a deuterated FeO surface and adjacent water molecules.⁶⁵ It has previously been shown using our reactive interatomic potential, which is also employed here, that bridging oxygens with Si–O–Si angles in the 125 to 135 degree range, substantially more acute than bulk silica's mean siloxane angle of 150 degrees, can host metastable protons.⁵⁷ This is consistent with *ab initio* calculations^{66,67} and seen in *ab initio* simulations of In- and Ga-phosphides forming bridging oxygen sites with an attached proton.⁶⁸ Similarly, silanol sites with an additional proton attached (SiOH₂⁺) seen in additional simulations²⁷ are also highly unstable and act as excellent transfer sites for protons. Such SiOH₂⁺ sites have been observed experimentally.⁶

Using *ab initio* calculations of water between quartz surfaces, Sulpizi *et al.*¹⁸ determine a difference in the H-bond lengths for in-plane H-bonds between surface sites *versus* out-of-plane H-bonds from the surface hydroxyl to the adjacent water in comparison to H-bond lengths in bulk water.

Takei and Chikazawa found that for hydrated porous silica glass (PSG) and quartz samples, from which they measured relatively high heats of immersion, the infrared spectra indicated a predominance of hydrogen-bonded surface hydroxyl groups.⁶⁹ By contrast, for aerosol and silica gel samples, for which they measured low heats of immersion, the IR spectra indicated an abundance of free hydroxyl groups, implying that different silica surface morphologies result in different adsorbed water structures.⁶⁹

In the current simulations, a robust reactive multibody potential is used to evaluate the atomistic structure and dynamics of water and H-bonds lifetimes and proton transfer at the amorphous silica surface in large-scale systems that accommodate a variety of surface sites that not available in computational studies of crystalline silica surfaces. This potential has been used, unchanged, in a variety of scenarios involving structural, thermodynamic, and dynamic properties and proton transfer that are consistent with *ab initio* calculations and experiment, showing significant transferability.^{25–27,33,38,55–57,70–72}

For instance, while designed to match the density-temperature curve for bulk water, the potential generates bulk water structure based on the O–O spacing and first peak intensity consistent with the experimental data.^{73,74} Other predicted properties of bulk water include: the heat of vaporization is 10.4 kcal mol^{−1}, similar to experiment, the diffusion constant 2.4×10^{-5} cm² s^{−1}, similar to experimental data (2.3×10^{-5} cm² s^{−1}), a good frequency spectrum, and dipole moment of 2.6.⁷³

Upon exposing amorphous silica to water,^{27,56,57} the reactions created SiOH's at concentrations consistent with experimental data ($\sim 4\text{--}5$ nm^{−2}) and the types of sites consistent with experimental data (isolated, vicinal, germinal silanols and a small concentration of highly reactive SiOH₂ sites seen experimentally⁶ and in DFT calculations of water on oxide surfaces⁵⁹). Reactions on the silica surface included proton transfer to an adjacent H₂O molecule to form an H₃O⁺ ion that transferred the excess proton either to other waters or to a silica surface oxygen in mechanisms precisely consistent with *ab initio* MD simulations.^{27,56,58,59}

The potential was also used for nanoconfined water in amorphous silica, in which the simulations show the increase in the change in volume as a function of temperature for 7 nm pores and 3 nm pores consistent with the experimental data, with the addition of identifying the mechanism for the increased coefficient of thermal expansion observed experimentally for decreasing pore sizes.^{25,26}

Further simulations with this same potential showed proton transfer in bulk water *via* Eigen and Zundel complexes of the H₃O⁺ ion, with the transfer of a proton in the Zundel complex.³³ The simulations showed the decrease in the energy barrier to proton transfer with decreasing O–O spacing between the H₃O⁺ ion and an H₂O molecule in bulk water,³³ as predicted from quantum calculations;⁴⁰ the free energy barrier for proton transfer in a Zundel complex at O–O spacing of 2.4 Å with a value of 0.8 kcal mol^{−1} in our simulations,³³ consistent with Marx's *ab initio* value of 0.6 kcal mol^{−1} at 2.4 Å spacing using a classical proton.⁴⁰ Again, all without any change in the potential.

Computational procedure

The simulation was conducted using our own MD code that consists of a fifth order Nordsieck–Gear integrator and a reactive, all-atom potential consisting of two-body and three-body terms.^{56,57,73}

The system consists of a vitreous silica slab of 12 226 SiO₂ molecules (36 678 atoms) made from a melt/quench procedure performed using periodic boundary conditions (PBC) in three dimensions similar to previous work.²⁷ A β -cristobalite crystal

was melted at 6000 K and cooled to 300 K using intervening temperatures over 430 ps in constant number, volume, and energy calculations, with a timestep of 1 fs and a coefficient of thermal expansion of 5.5×10^{-7} . The x, y, z dimensions of the resulting glass were $\sim 104 \text{ \AA} \times \sim 104 \text{ \AA} \times \sim 50 \text{ \AA}$, respectively.

The glass surface was made by removal of the PBC in the z dimension and subsequent relaxation of the glass at elevated temperature with the lower 25 Å of the glass atoms frozen so as to retain the original bulk-like structure, similar to the original methodology of studying the water/glass interface.⁷⁵ The free surface was exposed to water, with the water/glass interface perpendicular to the z axis at $\sim 50 \text{ \AA}$ in z . The box size in the z dimension was increased to 125 Å, and 7300 water molecules (21 900 water atoms) were added, producing a water layer of thickness $\sim 20 \text{ \AA}$, with 56 Å of vacuum above the water. The resulting system contains 58 578 atoms. The configuration is shown schematically in Fig. 1a.

This system was equilibrated for 3 million steps (300 ps) at (NVE (constant number of atoms, volume, energy)), using a timestep of 0.1 fs to account for the presence of the protons. It was then run for 0.25 million steps (25 ps) in the NVT ensemble using a Berendsen thermostat with velocity rescaling every 10 timesteps at a constant temperature of 298 K, and continued for an additional 1 million steps (100 ps) at constant energy (NVE). The data presented here were obtained from this final NVE run. The temperature drift throughout the run was small, with a maximal temperature of 298.6 K and a final temperature of 298.4 K.

For our analysis, we employed the topological hydrogen bond (H-bond) definition proposed by Henchman, *et al.*^{76–80} and previously used by us for simulations of bulk water.³⁸ This H-bond definition has no distance or angle criteria. In particular, for every proton H, its nearest and second-nearest oxygen atoms are respectively labeled $O_1(H)$ and $O_2(H)$ (O_1 is the covalently bonded O to the H and O_2 is the H-bonded O to that H). According to the topological definition of the hydrogen bond, $O_1(H)$ and $O_2(H)$ are hydrogen bonded if there does not exist another hydrogen bond between $O_1(H)$ and $O_2(H)$ with shorter H-bond length. Thus, there can only be one hydrogen bond between a particular pair of oxygen atoms; if two protons

simultaneously claim the same pair of oxygen atoms as O_1 and O_2 (the protons may be covalently bonded to the same water molecule, or to opposite molecules- conditions 1 and 2, respectively, in Fig. 1b), then the proton with the shorter H- O_2 distance is deemed a bond-forming proton and the one with the longer H- O_2 distance is referred to as a dangling proton (see Fig. 1b). Every proton that is not dangling forms one H-bond. As we have previously shown in the simulations of bulk water, this criterion accurately discerns between protons which are and which are not geometrically and dynamically consistent with hydrogen bonding.³⁸

The system's oxygen atoms were considered glass surface oxygens in a given configuration if they were bonded to at least one silicon atom; otherwise, they were labeled water oxygens. A silicon and oxygen pair are regarded as bonded if their interatomic distance is shorter than 2.1 Å. The oxygen atoms in the glass were potentially bonded to one Si (terminal oxygens), two Si (bridge oxygens), or three Si (tricluster oxygen). However, the three-coordinated oxygens were uncommon on the surface, did not interact substantially with water, and were therefore discarded from the analysis.

Every oxygen atom in the water was labeled within a 'layer' according to its topological distance from the silica surface in the water's hydrogen bond network in a given configuration. Specifically, a W1 oxygen has a hydrogen bond with the silica surface, either with the H from the water molecule or from the surface silanol site, and is in layer 1; a W2 oxygen is hydrogen bonded to a W1 (but not to a surface oxygen) and is in layer 2; in general, a W_i oxygen is hydrogen bonded to a $W(i-1)$, but not to a surface oxygen or to a W_j for $j < i-1$. Finally, each proton was labeled according to the pair of labels assigned to its donor and acceptor oxygens. A group of protons is defined as X, Y where X is the label of the proton's donor oxygen and Y is the label of the proton's acceptor oxygen. A dangling proton is only labeled according to the label of its donor oxygen, since dangling protons do not form hydrogen bonds according to this nomenclature.

Several structural parameters were characterized as a function of proton label. In particular, r_i refers to the distance between a proton and its i -th nearest oxygen (hence r_1 refers to the covalent OH distance whereas r_2 refers to the O-H H-bond distance, and r_3 is the distance from the proton to its third nearest oxygen, *etc.*). $\delta(H)$ refers to $r_3 - r_2$. These quantities, as well as the angle distributions and dipole moment distributions, are presented as probability density functions with the area under all curves normalized to 1.

Dynamics were characterized *via* intermittent and continuous H-bond lifetime autocorrelation functions. Continuous autocorrelation functions measure the probability that a given hydrogen bond exists without any transient breaking from an initial time t_0 to a later time $t_0 + t$. Intermittent autocorrelation functions measure the probability that two molecules are hydrogen bonded at time t_0 and at $t_0 + t$, regardless of the H-bond state between those times. Both types of autocorrelation functions were calculated for all protons which had a specific label at time t_0 . A H-bond is also considered to remain intact if the proton transfer



Fig. 1 (a) Schematic drawing of system. (b) Conditions for describing H-bonds.

just causes the donor and acceptor oxygens to switch roles. Intermittent autocorrelation functions $C_i(t)$ and continuous autocorrelation function $C_c(t)$ are respectively given by the formulas:

$$C_i = \frac{\langle f(\text{H}, t_0)f(\text{H}, t_0 + t) \rangle}{\langle f(\text{H}, t_0) \rangle} \quad (1)$$

$$C_c = \frac{\langle f(\text{H}, t_0)F(\text{H}, t_0 + t) \rangle}{\langle f(\text{H}, t_0) \rangle} \quad (2)$$

where $f(\text{H}, t_0)$ is equal to 1 if a specified condition holds for proton H at time t_0 , or is equal to 0 otherwise. For C_i , $f(\text{H}, t_0 + t)$ is equal to 1 if the same specified condition that holds at t_0 also holds for proton H at time $t_0 + t$, regardless of the state between those two times, otherwise it is equal to 0; therefore, the product in the numerator, $f(\text{H}, t_0)f(\text{H}, t_0 + t)$, is equal to 1 for a proton H if the condition holds at both time t_0 and a later time $t_0 + t$, and is equal to 0 otherwise. For C_c , the product $f(\text{H}, t_0)F(\text{H}, t_0 + t)$ is equal to 1 if the specified condition at t_0 also holds continuously for proton H from time t_0 to a later time $t_0 + t$.³⁸

In our analysis of proton transfer (PT) events, a proton transfer is considered to occur between two configurations if the proton is closer to its first host O1 in the former configuration, and closer to its new host O2 in the subsequent configuration. Many such events consist of rattling, where the proton transiently transfers from O1 to O2, and returns back to O1 within femtoseconds, as previously discussed.³⁸

The calculation of proton energy barriers was similar to calculations previously described in detail,³³ and used in studies of corrosion of silica exposed to water.⁷⁰ Briefly, protons with a given pair of donor (O_a) and acceptor (O_b) oxygens were selected, and three sets of donor–acceptor (O_a – O_b) initial spacing were selected, 2.4 Å, 2.5 Å, or 2.6 Å. Previous *ab initio* calculations⁴⁴ and our MD simulations³³ showed a decrease in the barrier to PT with decreasing O_a – O_b spacing, as was also seen here. Since only the data for O_a – O_b spacing below 2.5 Å is relevant in comparison to previous data, only data from the 2.4 Å O_a – O_b spacing are presented. The initial donor–acceptor (O_a – O_b) spacing at each distance was within 0.01 Å of the specified distance. Potential of mean force (PMF) curves were calculated for these protons by fixing the O_a – O_b distance at 2.4 Å, as well as the O_d –H distance between the original donor and the proton using the RATTLE algorithm and the velocity Verlet integrator.⁸¹ The O_a –H distance was then increased from its original value to a target value of less than 1.1 Å from the accepting oxygen, O_a , in increments of 0.01 Å, indicative of a proton transfer. Each O_d –H distance was held for 10 000 steps (1 ps), and the force required to maintain this distance was averaged over the latter 5000 steps. These average forces, as a function of O_d –H distance, were integrated to obtain PMF curves, the peak heights of which were taken as the PT energy barriers.

Results and discussion

Structural data

The density profiles of the atoms in the system as a function of their z -coordinate are shown in Fig. 2a, with images of side

views of the system in Fig. 2b and c. The locations of the O in the water molecules are used to delineate the different water ‘layers’, based upon the nomenclature presented above. Only the first 7 ‘layers’ are depicted. As seen, protons penetrate at least 10 Å into the glass, either as those that have attached to a glass O (labeled H (SiO_2) in the figure) forming SiOH or SiOH₂ or as OH’s or H₂O’s and labeled H (water). As the figure shows, and assuming a Gibbs Dividing Surface of the glass at ~ 50 Å, water molecules in the W1 layer, which are H-bonded to the glass oxygens, are the dominant species in the first 3 Å adjacent to the glass. The density of the water in this location, also including part of the W2 layer, is also slightly higher than that farther from the surface. This is consistent with previous data that showed such a density increase at the interface that caused the enhanced thermal expansion in nanoconfined water.²⁵ Based on that previous work, this density increase is in the range of only $\sim 4\%$, which is sufficient to explain the expansion behavior²⁵ and is much less than the 20–50% density increases observed in simulations by others using the popular rigid (non-reactive) water potentials.^{82–86}

Images of the water/glass system is shown in Fig. 2b and c. Fig. 2b shows a side view of the full system with water (cyan bond color) on top in the z dimension and silica (blue and grey atoms and grey bonds) below. Some water molecules are seen to have penetrated into the glass. Fig. 2c provides a better view of this penetration of water into the silica. In Fig. 2c, only Si–O bonds from the outermost Si ($z > 49$ Å) and below 38 Å are shown as grey and only O from water below 49 Å are shown as cyan spheres. The figure shows penetration of water into the glass surface at room temperature caused by the presence of sufficiently large network rings of connected SiO tetrahedra that allow penetration.

The structural data in Fig. 3a–e show how the hydrogen bond geometry changes near the interface. The inset in Fig. 3a shows a schematic of the bonds specific to the r_i bond length nomenclature. The legend provides the labels for the location of the H bond, where 0 is a surface site, 1 is the W1 1st water ‘layer’ site, *etc.* The r_i values between two surface sites is therefore labeled 00 for the donor–acceptor pair, respectively, whereas the H-bond from a surface site to a W1 water molecule is labeled 01, while the reverse H-bond would be labeled 10; the H-bond between two W1 waters is labeled 11, and so forth. Distances obtained in simulations of bulk water are included. The r_1 distributions show that the covalent bond between the proton and its oxygen is slightly shorter for bonds between surface species (00 curve) and slightly longer between surface species and the first layer of water (01) than those bonds involving only water–water interactions in farther ‘layers’. These latter bonds are very similar to that of bulk water.

The r_2 distributions in Fig. 3b show a significant shortening of the position of the peak maximum in the H-bonds donated from the protons attached to O on the glass surface to the layer 1 (W1) waters (01 curve) in comparison to bulk water, similar to the *ab initio* calculations by Sulpizi *et al.*¹⁸ Also similar to their *ab initio* calculations is our result for the 00 (or what they call ‘in-plane’) H-bonds that are shorter than those between bulk

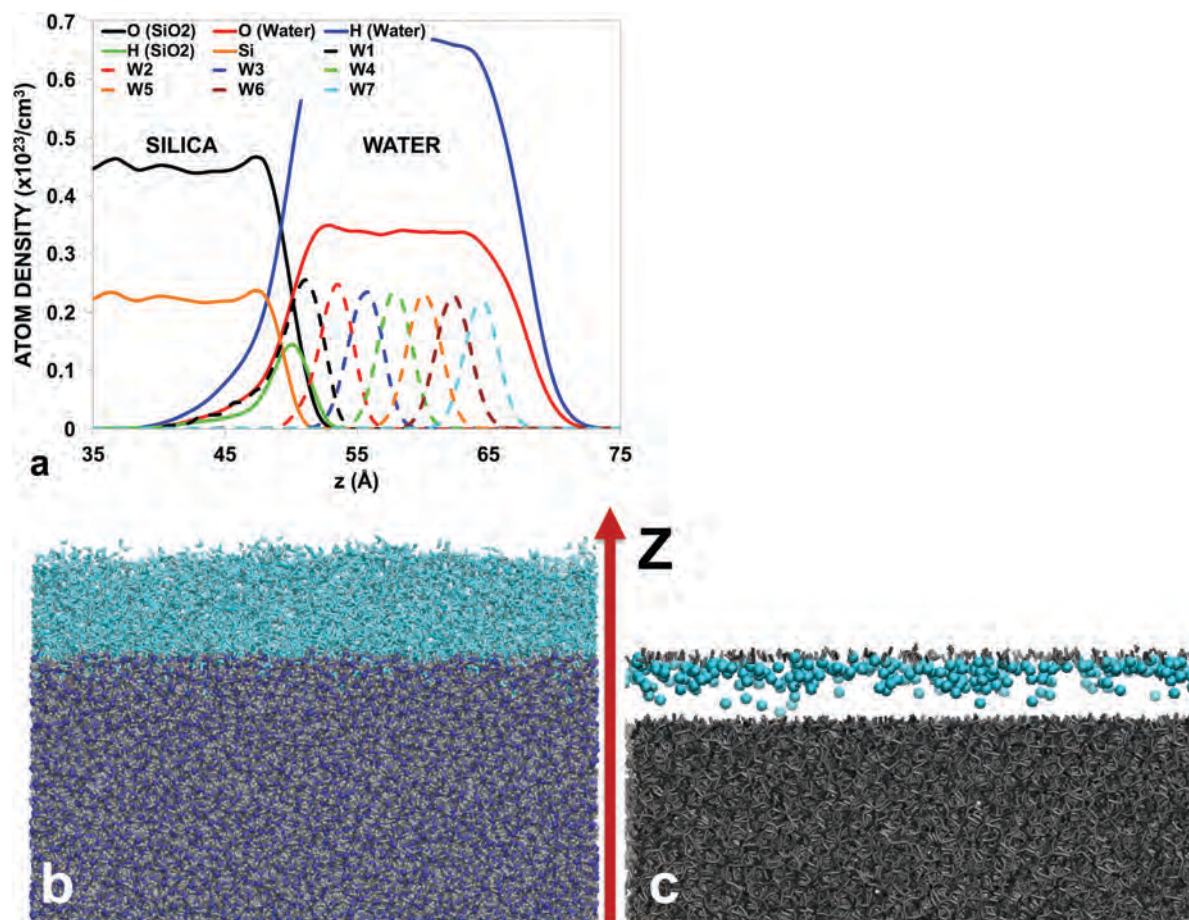


Fig. 2 (a) Density profiles of atoms in the glass and water; W_i indicate location of the O atoms in water as a function of water 'layer' based on H-bonding (see text). (b) side view of system with Si atoms in blue, SiO bonds in grey, and water OH bonds in cyan; (c) SiO bonds at $z > 49 \text{ \AA}$ and $z < 38 \text{ \AA}$ and water oxygen at $z < 49 \text{ \AA}$ shown as cyan spheres. (c) shows water penetrating 11 \AA below outer Si atoms at 300 K .

water and from water to the glass surface. However, because Sulpiza *et al.* used the quartz surface, the heterogeneity of the amorphous silica surface would not be accurately described. This is significant in affecting the calculation of H-bond lengths between the donating W_1 water and the surface sites since the smaller ring structures present on the glass surface that are not present on the quartz surface significantly affect the H-bond strength (length), as will be discussed below regarding H-bond reorientations and lifetimes.

The r_3 distributions in Fig. 3c show that H-bonds donated by surface sites and by W_1 molecules to the surface (00 and 10 curves, respectively) have next-nearest acceptors which are significantly closer than the next-nearest acceptors of bulk water H-bonds. Specifically, H-bonds accepted by surface sites (whether they are donated by a W_1 (10) or by another surface site (00)) have a modal next-nearest acceptor (r_3) distance of 2.6 \AA ; the typical range for the r_3 value for a linear H-bond in bulk water is 2.7 \AA to 3.2 \AA ³⁸ with a modal r_3 near 3.0 \AA . H-bonds donated by surface sites to W_1 molecules (01 curve) have a modal r_3 of about 2.65 \AA , and H-bonds donated by a W_1 to a W_1 have a modal r_3 of about 2.8 \AA . Beyond the W_2 layer, r_3 distances do not differ appreciably from those of bulk water values.

As can be seen in the δ distributions of Fig. 3d, this proximal O_3 pulls H-bonds which are accepted by surface sites into a bifurcated geometry (δ values near zero). Notably, even though H-bonds donated by surface sites to W_1 (01) have down-shifted delta peak locations compared to bulk water H-bonds, only H-bonds accepted by surface sites (00, 10) have enhanced probabilities of near-zero δ values which imply substantial populations of bifurcated H-bonds. As with other structural parameters, δ distributions of H-bonds beyond the W_2 layer closely follow those of bulk water and are not shown.

The notable proximity of the second acceptor molecule (r_3 curves) and near zero value for the difference in the distances between the first and second acceptor oxygens for the proton shown in the δ curves for the (10) H-bonds indicates that despite having a decreased affinity for a particular acceptor relative to bulk water (as will be shown below in the correlation functions), water molecules in the W_1 layer are stabilized by their protons' close attractive interactions with multiple local surface acceptor sites. Combined with the decreased r_3 values of the surface–surface H-bonds (00), indicating vicinal H-bonds between surface sites, the results are consistent with the increased values of the heats of immersion observed experimentally for those silica surfaces

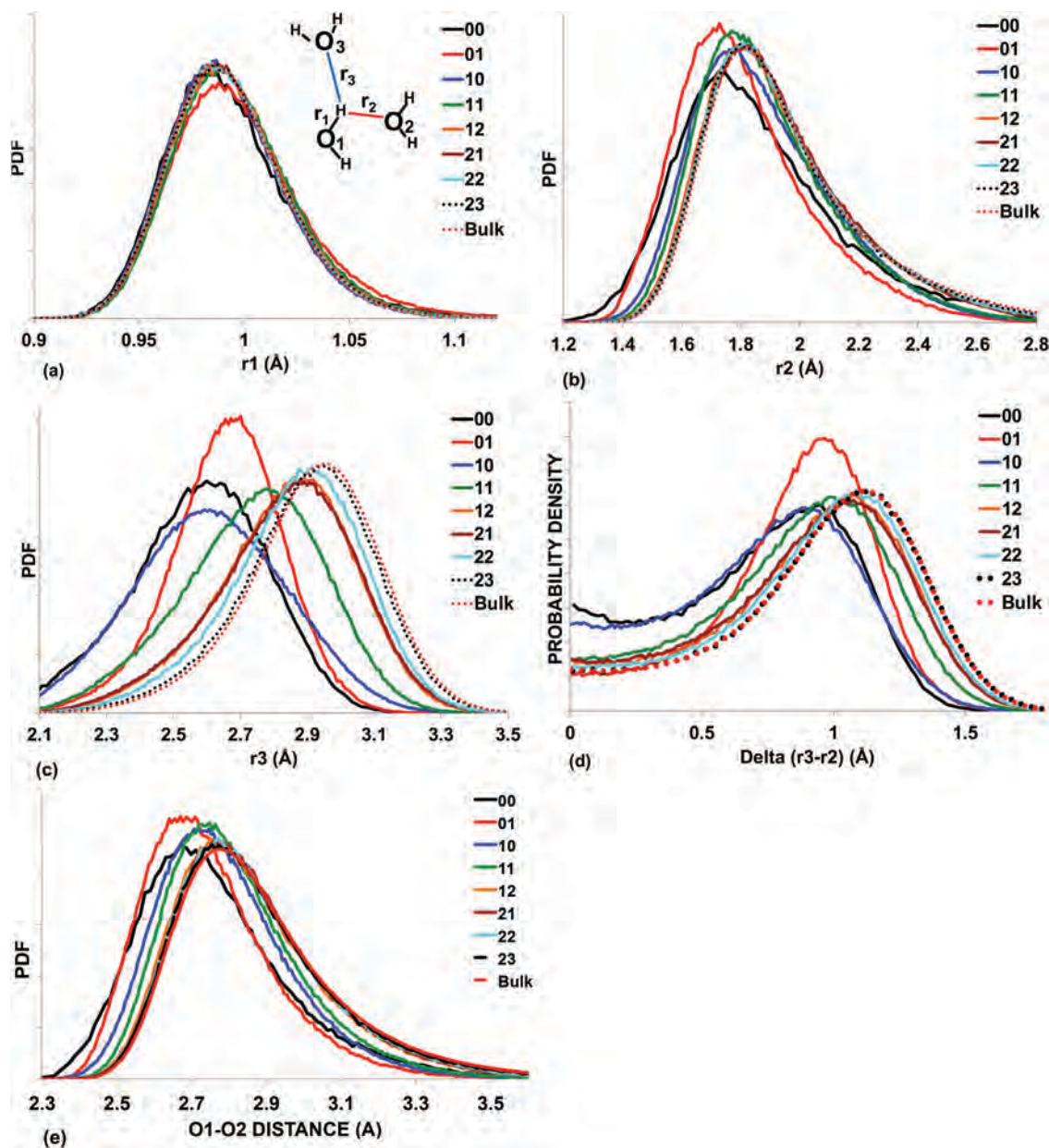


Fig. 3 H–O distances for different locations of donor–acceptor pairs at: (a) r_1 ; (b) r_2 ; (c) r_3 ; (d) $r_3 - r_2$ difference; (e) O1–O2 distance. r_1 , r_2 , r_3 labels given in inset in (a). See text for legend.

that have increased vicinal silanols⁸⁷ versus those silica surfaces containing predominantly only isolated silanols.

The combined results of shorter r_2 H-bond distances and r_3 distances for the surface (00) and interface H-bonds (01, 10, and 11) imply stronger bonding between water at the interface in comparison to bulk water which also correlates with the heat of immersion data of Takei *et al.*⁸⁷

The shortening of the H-bond r_2 lengths shown in Fig. 3b can be correlated to the shortening of the O1–O2 distances shown in Fig. 3e, in which O1 is the covalently bonded O to the proton and O2 is the H-bonded oxygen to the proton. The figure shows that H-bonds donated by surface sites have the closest O1–O2 spacings, followed by the H-bonds donated by W1

molecules to surface sites and to other W1 molecules. H-bonds involving W2 molecules and beyond do not differ appreciably from bulk water O1–O2 spacings. The shortened O1–O2 spacing is especially relevant to proton transfer; a decrease in the O1–O2 spacing in water shows a decrease in the energy barrier to proton transfer, as was seen in our previous MD simulations of proton transfer in the H_3O^+ ion in bulk water²⁷ and is consistent with *ab initio* calculations.^{44,88}

The $\text{O}_2\text{--O}_1\text{--H}$ angle distributions of Fig. 4a further elucidate the effect of proximal acceptors on the H-bonds accepted by surface sites. Only the H-bonds accepted by surface sites have appreciably widened $\text{O}_2\text{--O}_1\text{--H}$ angles compared to bulk water, further corroborating the notion that substantial numbers of

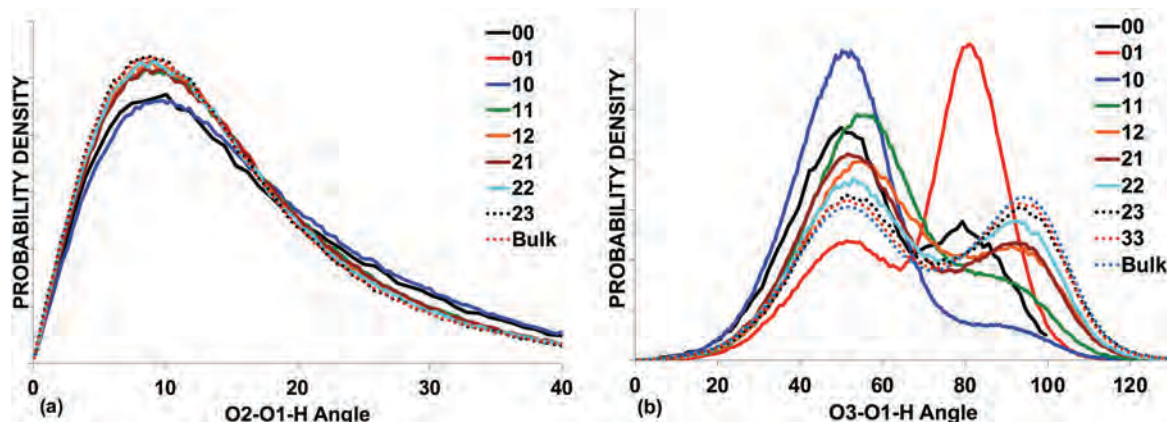


Fig. 4 Bond angles for O₂–O₁–H in (a) and O₃–O₁–H in (b) and provides location of proton's second acceptory O (see text). O_i given in Fig. 3a inset. Legend as in Fig. 3.

H-bonds accepted by surface sites adopt a bifurcated structure due to a proximal second acceptor. The O₃–O₁–H angles of Fig. 4b clarify the nature of these proximal acceptors. As previously demonstrated,³⁸ the wide-angle peak of this distribution corresponds to a next-nearest acceptor which is in the donor (O₁) oxygen's first shell, and the small-angle peak corresponds to a next-nearest acceptor which is in the acceptor (O₂) oxygen's first shell. W1-to-surface H-bonds (10 curve) have a very dominant small-angle peak, while surface-to-W1 H-bonds (01) have a very dominant wide-angle peak; in both cases, nearly all H-bonds have an O₃ that is attached to the surface site rather than to the water molecule. This leads to bifurcated geometry in the case of W1-to-surface H-bonds because a proton can more easily access a next-nearest acceptor bonded to its acceptor oxygen than one bonded to its donor oxygen. This is discussed further below. The water layers farther from the surface and bulk water show equal distributions of both peaks, as does water.

Distributions of angles between molecular dipole moments and the +z-axis as a function of the z position of the O in the water molecule in Fig. 5a and the average angle for each layer as

a function of the average z position of the water molecules in that layer in Fig. 5b. As expected, a very strong orientational anisotropy extends from the surface to the vacuum, which begins near layer W9. The large variations in the angles in Fig. 5a below 50 Å and near 70 Å in the z location are due to the small number of water molecules that enter the glass subsurface in the former and at the water/vacuum interface in the latter. The low concentration of water molecules in these locations can be inferred from the density profiles in Fig. 2.

Evaluation of these dipole angles to the +z axis separated into the specific 'layers' in Fig. 5b shows that the first five water layers have a modal orientation that is strongly aligned with the z-axis in the direction of the silica surface, decaying toward a more random distribution of angles (90°) that would be similar to the bulk water. The slope of the value of the dipole orientation with respect to the +z axis is high for the first 5 'layers' shown in Fig. 5b, decaying beyond that, again indicating the extent of the strong anisotropy near the interface. There is no significant variation in the magnitude of molecular dipole vectors at the interface; only the orientation is correlated with layer.

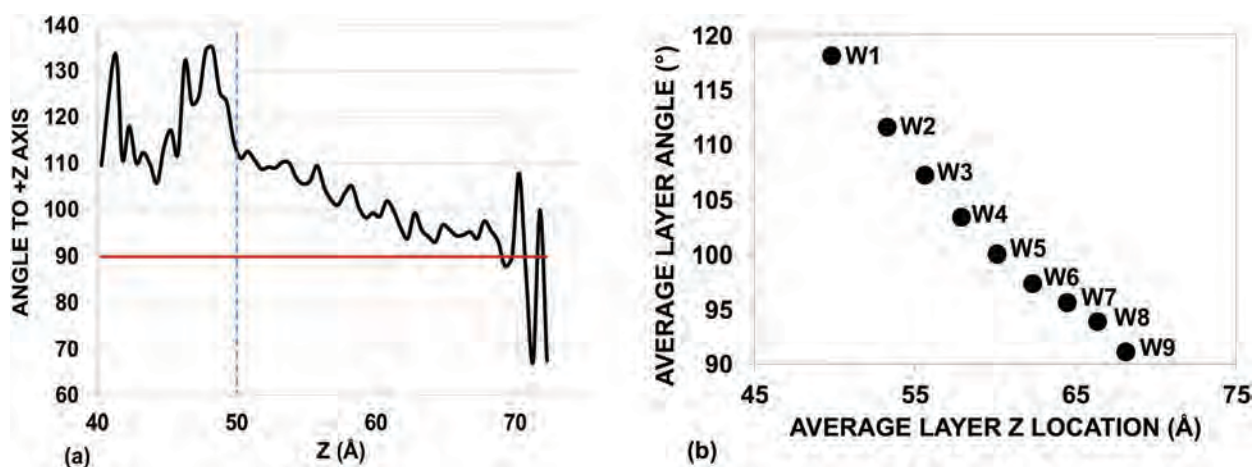


Fig. 5 (a) Dipole moment orientation of water molecules related to the +Z axis direction. Vertical dashed line indicates approximate location of glass surface. (b) Average angle of the dipole moment relative to the +Z axis for each water 'layer'.

Topologically, the dipole moment orientation near the interface takes the form of H-bonding directionality. Due to the vast surplus of acceptor sites on the surface, and to the limited scale of protonation, 92.6% of H-bonds between bridge sites and water molecules are accepted by the bridge site, and 58.3% of H-bonds between terminal sites and water molecules are accepted by the terminal site. 68.7% of H-bonds between W1 and W2 molecules are accepted by the W1; this imbalance drops off slowly, with 66% of W2/W3 H-bonds accepted by the W2, and evening out by 2% to 3% per layer until the water-vacuum interface. Thus, the great surplus of acceptor sites at the interface has a profound, long-range effect on the H-bond network topology away from the interface.

Proton transfer barriers

Using potential of mean force (PMF) calculations similar to previous work,⁷⁰ the energy barriers to proton transfer (PT) as a function of the O–O spacing involving the excess proton on surface sites and barriers between water averaged over several different water ‘layers’ were determined. Consistent with previous *ab initio* calculations and our previous simulations of PT in the H_3O^+ complex involving Eigen and Zundel configurations,^{33,44} there is a decrease in the barrier to PT with a decrease in the O–O spacing between the donor oxygen and the acceptor oxygen. For O–O spacing of 2.4 Å, PT of the excess proton between surface sites had an average barrier of 0.80 kcal mol⁻¹; PT occurring between water molecules in W1 had a value of 1.15 kcal mol⁻¹, also at 2.4 Å, whereas PT in water layers W2–W5 had an average value of 1.71 kcal mol⁻¹ (see Fig. 6).

Our previous simulations gave a barrier to PT in the H_3O^+ complex in bulk water of 0.8 kcal mol⁻¹ for the O–O spacing in the Zundel complex at 2.4 Å,³³ similar to the *ab initio* result of 0.6 kcal mol⁻¹.⁴⁴ In the current simulations involving the silica interface, the barrier for H_3O^+ complex in W1 transferring its proton to a surface sites at 2.4 Å was 0.26 kcal mol⁻¹, considerably lower than that in bulk water. This very low barrier to PT from the H_3O^+ ion in the water adjacent to the glass surface would decrease the lifetime of the H_3O^+ ion and is consistent

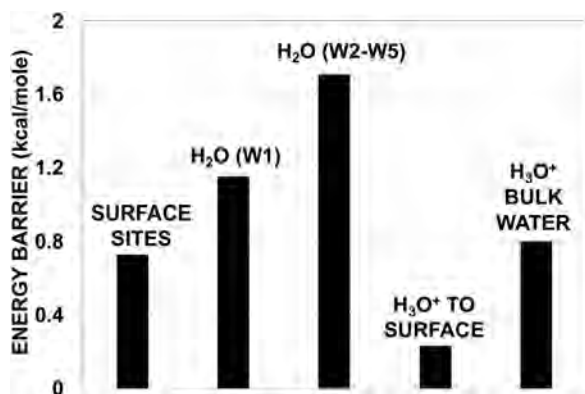


Fig. 6 PMF calculations of the average energy barriers to proton transfer for transfer between silica surface sites, neutral water molecules in W1 and in W2–W5 ‘layers’, H_3O^+ ions in W1 transferring to a surface site, and H_3O^+ ions transferring protons in bulk water, all at 2.4 Å O–O spacing.

with earlier simulations that showed such lifetimes are significantly reduced for H_3O^+ ions adjacent to the glass surface in comparison to H_3O^+ ions in bulk water.²⁷

The important implication of the data is that PT between surface sites and from H_3O^+ ions in the W1 layer to the surface all have lower barriers than in bulk water such that transfers among these sites would provide useful pathways for proton migration, especially under an electric field, as relevant in the electrochemical studies.^{28–31}

H-bond reorientation and lifetimes

The behavior of the H-bond network in water affects multiple processes and the dynamics involve H-bond reorientation and rupture. The lifetime of the H-bond is important in the initial proton transfer event in bulk water, as previously shown,³⁸ and H-bond lifetimes play an important role in the formation and structural diffusion of the H_3O^+ complex in bulk water.^{38,53} While the simulations showed that the longer H-bond lifetimes enhanced initial proton transfer between participating waters, forming ions, the rupture of this H-bond after a proton transfer event between these participating oxygens is extremely important for enabling the diffusion of an excess proton away from the initial event site.⁵³ Otherwise, mere proton rattling ensues. The rupture of the H-bond requires reorientation of the molecule. As discussed by Fayer *et al.*,⁸⁹ reorientation of a water molecule in bulk water involves penetration of a second shell water into the first shell, enabling H-bond rupture and reorientation with a jump angle of $\sim 60^\circ$, consistent with ideas discussed by Laage and Hynes.^{90,91} The role of the second shell water entering the first shell was shown in our previous simulations of bulk water, creating bifurcated H-bonds and the large jump reorientations.³⁸ According to Fayer, the number of first or second shell waters at an interface is restricted by the adjacent surface, reducing the probability of penetration by a second shell water and the number of large jump reorientations.⁸⁹ However, atomistic details at the amorphous silica surface have not been previously determined.

Evaluation of the angular displacement of the OH vector to the acceptor of the H-bond as a function of time for water molecules in various layers is given in Fig. 7 for sub-ps behavior in (a) and the multi-ps timeframe in (b). Water in W1 show the largest librational angle displacement within 50 fs (Fig. 7a), but crosses over to smaller displacements within ~ 170 fs. At long times, water molecules farther from the interface show the large average angular jumps similar to bulk water, but water at the interface show smaller reorientation jumps or angular displacements in comparison to bulk water.

These H-bond reorientations are concomitant with H-bond lifetimes. H-bond intermittent (C_i) (solid lines) and continuous (C_c) (dashed lines) lifetime autocorrelation functions as a function of the donor molecule’s layer for waters in layers 1 to 5 and bulk water are shown in Fig. 8a. In Fig. 8b, the same autocorrelation functions are shown for the proton on silanol sites (SiOH) or for the excess proton on a donor oxygen’s location on the bridge (siloxane) site or the silanol (SiOH₂) site. In all cases, the continuous lifetime autocorrelation functions decay more rapidly than the intermittent functions. In Fig. 8a, the continuous autocorrelation

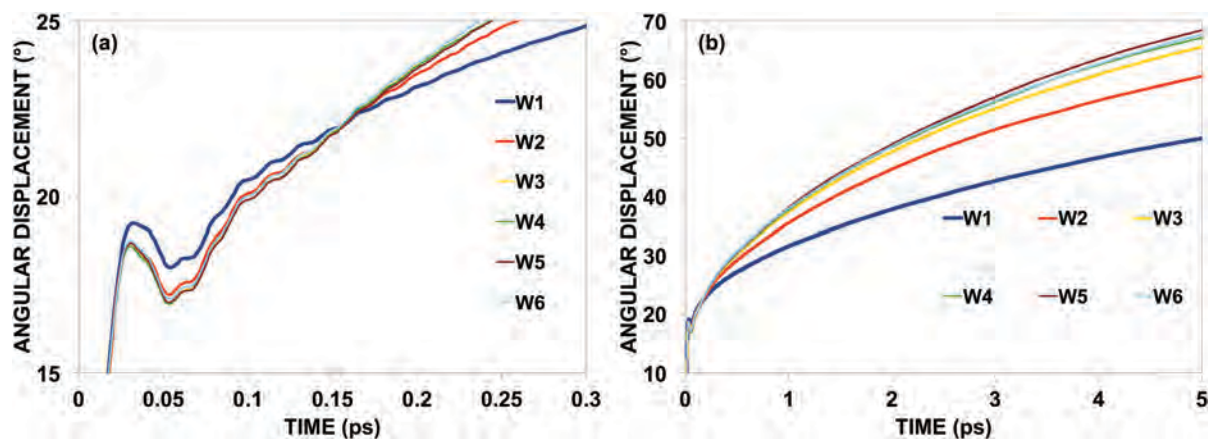


Fig. 7 Angular displacement of the OH vector to the acceptor O for the donor and acceptor oxygens in the given water layers for sub-ps time in (a) and multi-ps time in (b).

functions of W1 and W2 molecules decay more quickly than those of bulk water, indicating that interfacial H-bonds are less likely to survive continuously on these timescales. Farther from the interface, the hydrogen bond lifetimes in water layers W3 to W5 behave similar to bulk water. Oppositely, the intermittent H-bond lifetime autocorrelation functions shown in Fig. 8a for the W1 and W2 waters last considerably longer than bulk water, while water in W3–W5 behave similar to bulk water. Fig. 8b shows that the lifetimes of the H-bond of the terminal sites and bridge sites are considerably longer than those on water molecules, regardless of whether the water is in an interfacial ‘layer’ or bulk water.

The difference between the continuous and intermittent lifetimes and the longer lifetimes in water near the interface have important implications in behavior. The long intermittent H-bond lifetimes for water at the interface (W1) in comparison to their continuous lifetimes can be visualized in Fig. 9, in which the relevant oxygens O1, O2, and O3 to one of the protons in the water molecule are labeled in Fig. 9a. The numbers in Fig. 9 give the H–O_i interaction distances in angstroms, showing 2 normal

H-bonds between the 2 protons in the water molecule and their respective O2 oxygens in the glass surface in this particular moment in time, as well as the distance to one proton’s O3 oxygen.

The shorter continuous H-bond lifetime for W1 waters is caused by the reorientation of the water molecule from a proton’s O2 to its O3, as shown from Fig. 9a and b. The longer intermittent lifetimes for W1 in comparison to bulk water indicate that while the proton in a particular H-bond to an acceptor oxygen O2 can break that H-bond over a short time by switching to another acceptor oxygen O3 (Fig. 9b) ending the continuous autocorrelation function, that proton returns back to its original O2 within a short time (in this case, 500 fs), as shown in Fig. 9c. These oscillations of this particular proton between its original O2 and O3 oxygens continued for many ps. The silica surface provides O2 and O3 oxygens that have an average spacing of 2.6 Å, which is the normal first O–O distance in silica, with oscillations to shorter distances. This spacing is less than that between oxygens in bulk water (which is closer to 2.8 Å), and are considerably less mobile, thus enabling more reorientations of the H-bond between these relatively close surface oxygens.

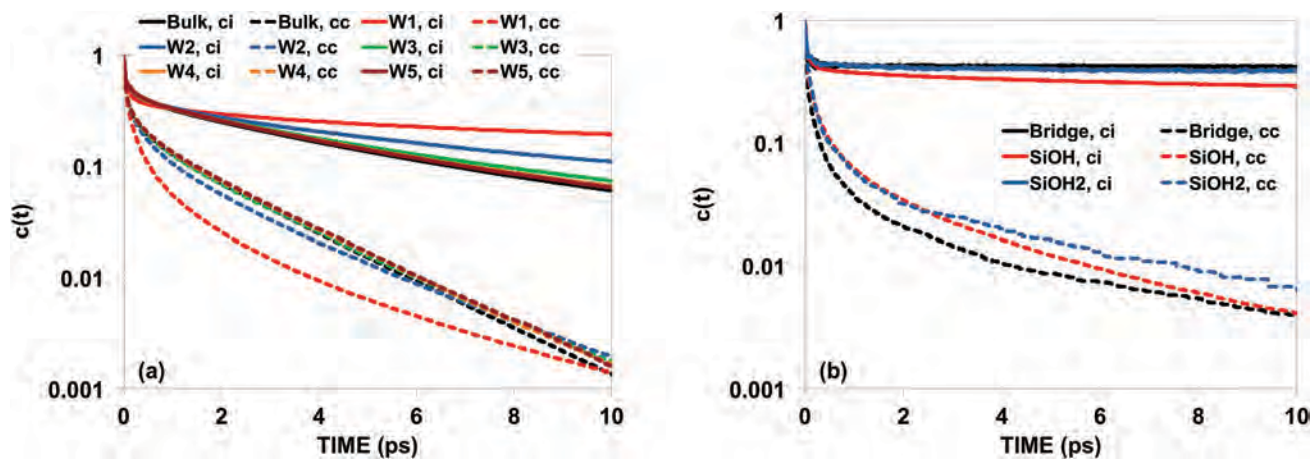


Fig. 8 Intermittent (ci, solid lines) and Continuous (cc, dashed lines) H-bond lifetime autocorrelation functions for (a) bulk water and water molecules in ‘layers’ W1 to W5; and (b) for protons on glass sites. Interfacial waters have longer ci than bulk water but shorter cc. Surface sites have both types of lifetimes longer than water.

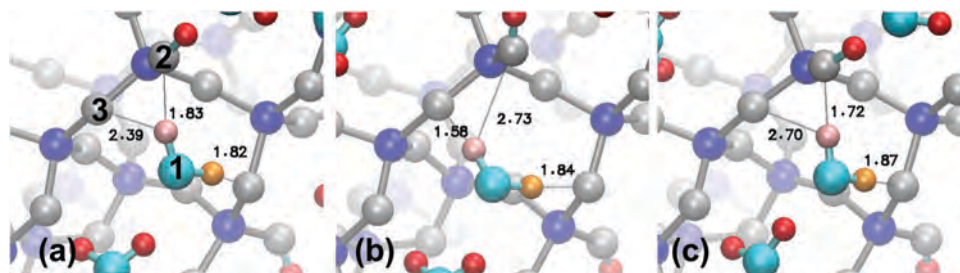


Fig. 9 Snapshots showing how Cc can decay rapidly for a particular H-bond, but not so with Ci. (a) H-bond present between O1 (labeled 1) in a W1 water and O2 (labeled 2) at an SiOH site, which switches in (b) to form a new H-bond to O3, returning to O2 in (c). This continued for many ps. The lower (gold) proton retained its H-bond to its O2 that is a bridging oxygen. O labels given in (a) and numbers are H-bond lengths in Å. Si = blue, O = grey on Si, O from water = cyan, relevant H = pink and gold, other H = red.

The other proton on the water in Fig. 9 retained its H-bond to the bridging oxygen for most of the run, acting as a stabilizing anchor for the water molecule. As shown in Fig. 10, its peak maximum bond length is 1.70 Å, shorter than the common H-bond length in water (1.8 Å). It turns out that this bridging oxygen was at an Si–O–Si site that had a bond angle in the 125°–133° range. *ab initio* calculations^{66,67} and our previous simulations⁵⁷ showed that a proton is stabilized on bridges with such low siloxane bond angles. Here, the proton does not actually dissociate from the water molecule and attach to the bridging oxygen, but the low angle appears to enable a relatively stable H-bond to the site. The bridge angle on the O labeled 3 in Fig. 9a is closer to 150° and is therefore a less stable site for the H-bond.

Using heterodyne-detected vibrational sum frequency generation (HDVSFG) spectra, Urashima *et al.* showed that the 2 protons on a water molecule in contact with the silica surface have asymmetric H-bonds.⁹² They assumed one was to the silica surface and the other to waters pointing away from the surface. Another interpretation is also possible. An example of such a variation in the H-bonding can be shown with respect to the water molecule shown in Fig. 9. Fig. 10 shows the H–O distance between the 2 protons and their respective O2 oxygens. The figure clearly shows that the lower (gold) proton's H-bond (labeled 2 in the inset image in Fig. 10) is shorter than the other H-bonds from the upper (pink)

proton (labeled 1 and 3 in the inset). Fig. 10 shows that the upper proton shows longer H-bonds that cross between 1 and 3, consistent with the rotation shown in Fig. 9 and also providing another explanation of the HDVSFG data.

The slowed dynamics in the first layer which approach the bulk behavior in farther layers from the interface are consistent with NMR results from which Totland *et al.* inferred that approximately one layer worth of water at the surface is bound and that the remainder is free.⁹³ Such longer H-bond lifetimes in water adjacent to the silica surface enhance proton exchange between the donor and acceptor oxygens, as pointed out in previous simulations of proton transfer in bulk water³⁸ and shown next.

Proton transfer

This localization of the water molecules adjacent to the glass surface is also consistent with the reduced diffusion of water near glass surfaces.^{27,55} This retention of water molecules at the interface (W1) enables formation of longer-lived H-bonds that enable increased proton transfer. Fig. 11 shows the number of proton transfers as a function of the location of the donating and accepting oxygen in the surface or water layer. Any rattling of the proton between a particular oxygen pair is only counted once for each oxygen pair. Rattling means that a proton simply moves back and forth between the same two oxygen sites a

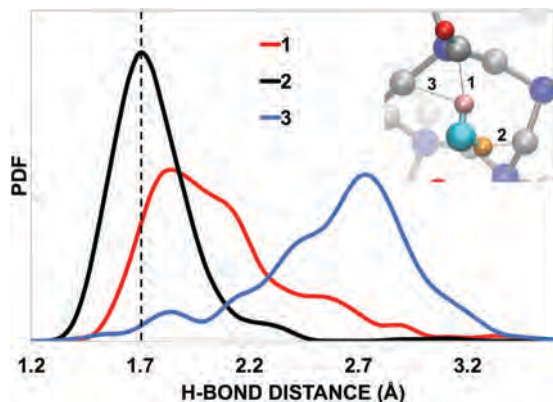


Fig. 10 Labeled H-bond lengths for H₂O molecule shown in inset and Fig. 9 showing asymmetric H-bonds. H-bond labeled 2 shorter than normal H-bond in water (1.70 Å peak max) vs. (1.8 Å for water).

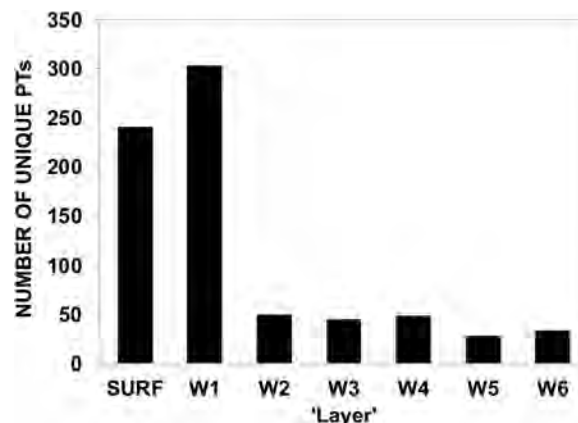


Fig. 11 Number of proton transfers involving O as a function of the location of the oxygen, either as the donor or the acceptor.

significant number of times in the run. Therefore, the number of proton exchanges given in Fig. 11 do not count these multiple rattles. Results clearly show that there are a significantly larger number of proton transfers occurring in the surface sites and W1 sites in comparison to all other layers. Such results are also consistent with the aforementioned free energy barriers to proton transfer and lifetime autocorrelation functions of the H-bond. If rattling were included in the data, the number of PT's occurring in the surface would be a factor of 25 higher and W1 would be a factor of 10 times higher than the data shown in Fig. 10, whereas the values shown for W2 to W6 would only be a factor of 3 times higher. Thus, there is a significantly higher number of proton rattles between sites at the interface in comparison to water away from the interface. This is consistent with the higher concentration of longer-lived H-bond lifetimes shown in Fig. 8. The longer the H-bond is retained between an H-bonded pair of oxygens, the higher the probability of the spacing between the oxygens fluctuating to a small distance, lowering the barrier to proton transfer, enabling PT. Again, the decrease in the O–O spacing involving the H-bond lowers the barrier to proton transport, as seen in previous MD simulations and *ab initio* calculations. However, the longer lifetime of the H-bond between these oxygens enables the proton to return to its original O, thus enhancing rattling.

H_3O^+ formation and structural diffusion

Fig. 12 shows proton transfer from a surface site to a W1 water followed by ion rotations and further transfer. Fig. 12a shows the initial configuration of a non-dissociatively chemisorbed H_2O molecule onto an originally 3-coordinated surface Si and its H-bond to a W1 water (numbers in the figure indicate specific O–H interaction distances with the red proton in angstroms). Fig. 12b shows some later time after proton transfer, showing the initial H_3O^+ ion, followed by rotation of the H_3O^+ ion (Fig. 12b and c), with additional structural diffusion of the H_3O^+ complex to form a new H_3O^+ ion in Fig. 12d. The rotational angle from Fig. 12b and c is $\sim 80^\circ$. The original transferring proton is red, but another proton from this initial H_3O^+ ion in Fig. 12b is transferred in Fig. 12d to form the second H_3O^+ ion. The other green spheres are O in water molecules that eventually become O in H_3O^+ ions, showing that additional structural diffusion of the H_3O^+ complex occurs.

This structural diffusion of the H_3O^+ complex away from the initial proton transfer site is important in providing an atomistic view of the interpretations of proton conduction in electrochemical studies of wet mesoporous silica.^{29,94} Those authors consider a 2-state model for the water, requiring a chemisorbed water layer and a physisorbed layer in which the physisorbed layer must be available to take a transferring proton away from

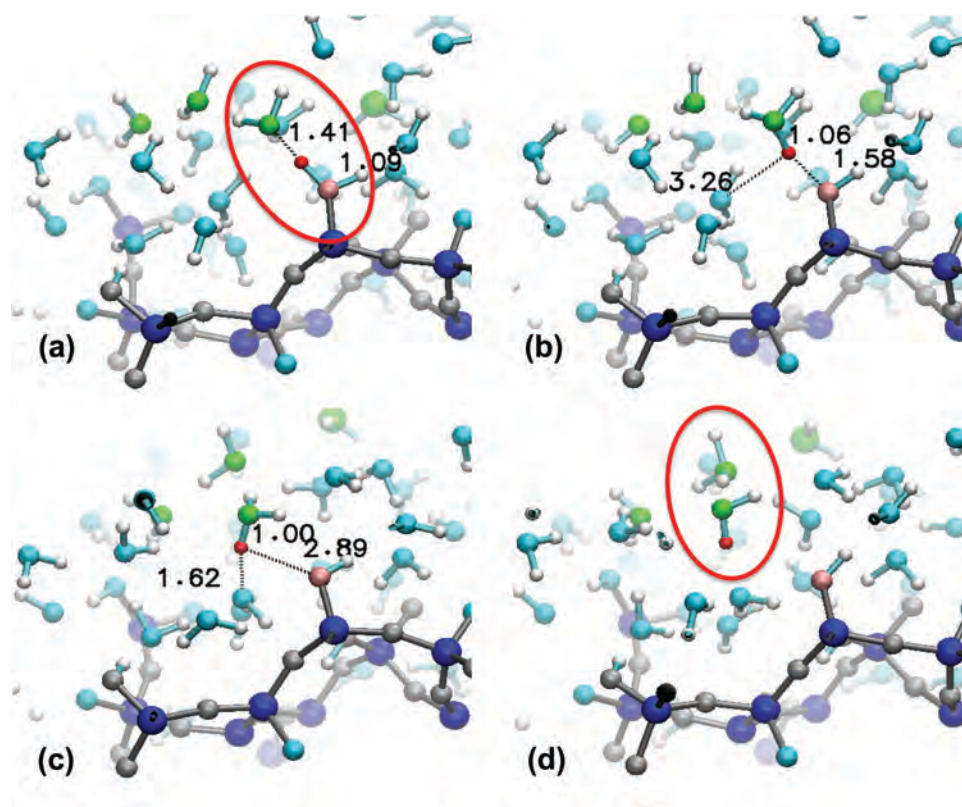


Fig. 12 (a) H-bond between a non-dissociatively chemisorbed water onto a 3-coordinated Si with a W1 water (red oval), with the relevant proton in red and the numbers giving O–H interaction distances; (b) proton transfers, forming the first H_3O^+ ion; (c) the H_3O^+ ion rotates away from the original H-bond site forming a new H-bond to a water molecule, followed by (d) transfer of an excess proton from this first H_3O^+ ion to form a new H_3O^+ ion (red oval). Green spheres are O in water that eventually become O in H_3O^+ ions, showing significant structural diffusion of the H_3O^+ complex. Si = blue, grey = O originally on Si, O from water = cyan, H = white, O chemisorbed on Si in (a) = pink.

the interface and into waters farther from the surface in order to enhance proton conductivity.

While our results confirm such an interpretation, in the majority of interfacial PT events of an excess proton from a surface site to a W1 water, we observed no rotation and breaking of the H-bond after the transfer. In these cases, rattling of the proton between the two participating oxygens occurred without subsequent structural diffusion.

Conclusions

Using a highly robust and reactive all atom potential that has previously been shown to reproduce multiple water properties and proton transfer consistent with experiment and *ab initio* data, the simulations provide detailed analysis of the behavior of water at a large-scale amorphous silica surface that shows the heterogeneity of surface sites and water/silica interactions that are missing in studies of crystalline silica surfaces and/or non-reactive water models.

Consistent with previous *ab initio* calculations, the simulations show a decrease in length of the H-bonds donated by protonated surface sites to the closest water molecules and to other surface sites in comparison to H-bond lengths in bulk water. The simulations also show that the water molecules donating H-bonds to the silica surface have H-bond lengths shorter than those in bulk water (although not as short as in the reverse H-bond from the surface to the water). The latter result was not detected in a previous *ab initio* calculation that used a quartz surface. However, the crystal surface lacks the heterogeneity of structures present in the glass surface such as smaller Si–O–Si siloxane bond angles that offer sites for stronger H-bonds. Consistent with HDSFVG data that indicate an asymmetry of a water molecule's H-bonds at the interface (assumed to be due to one H-bond to the surface and one H-bond to water), the simulations show a similar asymmetry but also show that it can be caused by an asymmetry of the two H-bonds to the glass surface.

The energy barrier to proton transfer at the interface (surface sites and W1 waters) is lower compared to that of water farther from the interface, allowing for an enhancement of proton conductivity seen in electrochemical studies. Contrasting this, however, is the considerably lower barrier to proton transfer from the H_3O^+ ion adjacent to the glass surface in comparison to that in bulk water. Such a low barrier would readily allow return of a newly accepted proton from the glass surface back to the surface site if the H-bond is not ruptured quickly. This highlights the important relation between H-bond lifetimes and proton transport.

W1 waters (those H-bonded to the silica surface) show opposite behavior with respect to the continuous *versus* the intermittent H-bond lifetime auto-correlation functions in comparison to bulk water and water farther from the interface. The continuous H-bond lifetimes of W1 waters are shorter than those in bulk water but the intermittent lifetimes are longer. This means that a W1 water breaks the H-bond to an accepting surface oxygen atom (O2) in a relatively short time, but remains localized to adjacent

surface oxygens and returns back to this original O2, reiterating this behavior over long times. This is also reflected in the relatively smaller angular displacements of the H-bond in W1 waters in comparison to bulk water.

These results show that rotations and rupture of a H-bond to a specific acceptor O on the glass surface occurs readily (faster than in bulk water and with smaller angular displacements). However, over long periods of time, these W1 waters remain at the local surface site. These observations provide additional information regarding the role of any interface with water on reducing the probability of H-bond rotations because of a lack of sufficient water molecules surrounding a central water near the interface in comparison to bulk water.

One can then apply this to proton transport *via* formation of a H_3O^+ ion in a W1 water from a proton on the glass surface. If the H-bond between that surface site and the newly formed H_3O^+ ion is not broken, the probability of return of the proton is high due to the very low energy barrier and proton transport is limited. Results showed such rattling in the number of proton transfers that is considerably greater at the interface than farther from it. However, the simulations also showed that breaking this H-bond between the H_3O^+ ion in W1 and the surface site enabled eventual proton transfer to waters farther from the interface. This rupture of the original H-bond occurred with formation of a new H-bond to an adjacent W2 water that eventually allowed the H_3O^+ ion to transfer an excess proton to water farther from the interface. This is consistent with the interpretations of electrochemical studies that discuss the need for a 2-state (or 3-state) model for water at the glass surface that enables enhanced proton conductivity.

In conclusion, the ability to use an interatomic potential that allows for proton transfer offers new details not available in simulations using non-reactive water potentials or crystalline surfaces. The simulations presented here show results consistent with *ab initio* calculations and interpretations of experimental data, but also provide specific atomistic mechanisms that provide a more robust picture of the behavior and reactions of water at the amorphous silica surface.

Conflicts of interest

There are no conflicts to declare.

Acknowledgements

The authors acknowledge support from the National Science Foundation (NSF) Environmental Chemical Science Program of the Division of Chemistry, grant number 1609044.

References

- 1 H. Le Roux, *Proc. R. Soc. London, Ser. A*, 1965, **286**, 390–401.
- 2 S. M. Wiederhorn, H. Johnson, A. M. Diness and A. H. Heuer, *J. Am. Ceram. Soc.*, 1974, **57**, 336–341.
- 3 B. C. Bunker, D. M. Haaland, T. A. Michalske and W. L. Smith, *Surf. Sci.*, 1989, **222**, 95–118.

- 4 T. Michalske and S. Freiman, *Nature*, 1982, **295**, 511–512.
- 5 T. A. Michalske and B. C. Bunker, *J. Appl. Phys.*, 1984, **56**, 2686–2693.
- 6 Y. Duval, J. A. Mielczarski, O. S. Pokrovsky, E. Mielczarske and J. J. Ehrhardt, *J. Phys. Chem. B*, 2002, **106**, 2937–2945.
- 7 H. E. Bergna, in *The Colloid Chemistry of Silica*, ed. H. E. Bergna, Am. Chem. Soc., Columbus, OH, 1994, pp. 1–47.
- 8 A. V. Bandura, J. D. Kubicki and J. O. Sofo, *J. Phys. Chem. C*, 2011, **115**, 5756–5766.
- 9 A. Pelmenschikov, H. Strandh, L. G. M. Pettersson and J. Leszczynski, *J. Phys. Chem. B*, 2000, **104**, 5779–5783.
- 10 W. H. Casey, A. C. Lasaga and G. V. Gibbs, *Geochim. Cosmochim. Acta*, 1990, **54**, 3369–3378.
- 11 Y. Xiao and A. C. Lasaga, *Geochim. Cosmochim. Acta*, 1994, **58**, 5379–5400.
- 12 L. J. Criscenti, J. D. Kubicki and S. L. Brantley, *J. Phys. Chem. A*, 2006, **110**, 198–206.
- 13 P. J. Lezzi and M. Tomozawa, *Int. J. Appl. Glass Sci.*, 2015, **6**, 34–44.
- 14 A. K. Soper, F. Bruni and M. A. Ricci, *J. Chem. Phys.*, 1998, **109**, 1486–1494.
- 15 C. Hartnig, W. Witschel, E. Spohr, P. Gallo, M. A. Ricci and M. Rovere, *J. Mol. Liq.*, 2000, **85**, 127–137.
- 16 M. Sovago, R. K. Campen, H. J. Bakker and M. Bonn, *Chem. Phys. Lett.*, 2009, **470**, 7–12.
- 17 P. Kumar, S. Han and H. E. Stanley, *J. Phys.: Condens. Matter*, 2009, **21**, 504108.
- 18 M. Sulpizi, M.-P. Gaigeot and M. Sprik, *J. Chem. Theory Comput.*, 2012, **8**, 1037–1047.
- 19 F. M. Etzler, *Langmuir*, 1988, **4**, 878–883.
- 20 A. Kiwilsza, A. Pajzderska, M. A. Gonzalez, J. Mielcarek and J. Wasicki, *J. Phys. Chem. C*, 2015, **119**, 16578–16586.
- 21 E. W. Hansen, R. Schmidt, M. Stocker and D. Akporiaye, *Microporous Mater.*, 1995, **5**, 143–150.
- 22 S. Takahara, M. Nakano, S. Kittaka, Y. Kuroda, T. Mori, H. Hamano and T. Yamaguchi, *J. Phys. Chem. B*, 1999, **103**, 5814–5819.
- 23 A. Faraone, L. Liu, C. Y. Mou, P. C. Shih, J. R. D. Copley and S. H. Chen, *J. Chem. Phys.*, 2003, **119**, 3963–3971.
- 24 T. Tsukahara, W. Mizutani, K. Mawatari and T. Kitamori, *J. Phys. Chem. B*, 2009, **113**, 10808–10816.
- 25 S. H. Garofalini, T. S. Mahadevan, S. Xu and G. W. Scherer, *ChemPhysChem*, 2008, **9**, 1997–2001.
- 26 S. Xu, G. W. Scherer, T. S. Mahadevan and S. H. Garofalini, *Langmuir*, 2009, **25**, 5076–5083.
- 27 G. K. Lockwood and S. H. Garofalini, *J. Phys. Chem. C*, 2014, **118**, 29750–29759.
- 28 M. Nogami, H. Matsushita, Y. Goto and T. Kasuga, *Adv. Mater.*, 2000, **12**, 1370–1372.
- 29 Y. Daiko, T. Kasuga and M. Nogami, *Microporous Mesoporous Mater.*, 2004, **69**, 149–155.
- 30 Y. Daiko, T. Kasuga and M. Nogami, *Chem. Mater.*, 2002, **14**, 4624–4627.
- 31 L. Malavasi, C. A. J. Fisher and M. S. Islam, *Chem. Soc. Rev.*, 2010, **39**, 4370–4387.
- 32 N. Agmon, H. J. Bakker, R. K. Campen, R. H. Henchman, P. Pohl, S. Roke, M. Thämer and A. Hassanali, *Chem. Rev.*, 2016, **116**, 7642–7672.
- 33 G. K. Lockwood and S. H. Garofalini, *J. Phys. Chem. B*, 2013, **117**, 4089–4097.
- 34 C. Knight and G. A. Voth, *Acc. Chem. Res.*, 2012, **45**, 101–109.
- 35 T. Hofer, M. Hitznerberger and B. Randolph, *J. Chem. Theory Comput.*, 2012, **8**, 3586–3595.
- 36 M. E. Tuckerman, A. Chandra and D. Marx, *J. Chem. Phys.*, 2010, **133**, 124108.
- 37 D. Marx, A. Chandra and M. E. Tuckerman, *Chem. Rev.*, 2010, **110**, 2174–2216.
- 38 J. Lentz and S. H. Garofalini, *Phys. Chem. Chem. Phys.*, 2018, **20**, 16414–16427.
- 39 S. Woutersen and H. J. Bakker, *Phys. Rev. Lett.*, 2006, **96**, 138305.
- 40 D. Marx, *ChemPhysChem*, 2006, **7**, 1848–1870.
- 41 M. Eigen, *Angew. Chem., Int. Ed. Engl.*, 1964, **3**, 1–19.
- 42 N. Agmon, *Chem. Phys. Lett.*, 1995, **244**, 456–462.
- 43 D. Marx, M. E. Tuckerman, J. Hutter and M. Parrinello, *Nature*, 1999, **397**, 601–604.
- 44 D. Marx, M. E. Tuckerman and M. Parrinello, *J. Phys.: Condens. Matter*, 2000, **12**, A153–A159.
- 45 M. Tuckerman, K. Laasonen, M. Sprik and M. Parrinello, *J. Phys. Chem.*, 1995, **99**, 5749–5752.
- 46 M. Tuckerman, K. Laasonen, M. Sprik and M. Parrinello, *J. Chem. Phys.*, 1995, **103**, 150–161.
- 47 A. Chandra, M. E. Tuckerman and D. Marx, *Phys. Rev. Lett.*, 2007, **99**, 145901.
- 48 H. Lapid, N. Agmon, M. K. Petersen and G. A. Voth, *J. Chem. Phys.*, 2005, **122**, 014506.
- 49 K. J. Tielrooij, R. L. A. Timmer, H. J. Bakker and M. Bonn, *Phys. Rev. Lett.*, 2009, **102**, 198303.
- 50 D. Laage, G. Stirnemann, F. Sterpone and J. T. Hynes, *Acc. Chem. Res.*, 2012, **45**, 53–62.
- 51 H. K. Nienhuys, R. A. van Santen and H. J. Bakker, *J. Chem. Phys.*, 2000, **112**, 8487–8494.
- 52 C. P. Lawrence and J. L. Skinner, *J. Chem. Phys.*, 2003, **118**, 264–272.
- 53 P. L. Geissler, C. Dellago, D. Chandler, J. Hutter and M. Parrinello, *Science*, 2001, **291**, 2121–2124.
- 54 B. Grunberg, T. Emmler, E. Gedat, I. Shenderovich, G. H. Findenegg, H.-H. Limbach and G. Buntkowsky, *Chem. – Eur. J.*, 2004, **10**, 5689–5696.
- 55 S. Xu, G. C. Simmons, T. S. Mahadevan, G. W. Scherer, S. H. Garofalini and C. Pacheco, *Langmuir*, 2009, **25**, 5084–5090.
- 56 T. S. Mahadevan and S. H. Garofalini, *J. Phys. Chem. C*, 2008, **112**, 1507–1515.
- 57 G. K. Lockwood and S. H. Garofalini, *J. Chem. Phys.*, 2009, **131**, 074703.
- 58 Y. Ma, A. S. Foster and R. M. Nieminen, *J. Chem. Phys.*, 2005, 122.
- 59 R. Sato, S. Ohkuma, Y. Shibuta, F. Shimojo and S. Yamaguchi, *J. Phys. Chem. C*, 2015, **119**, 28925–28933.
- 60 M.-H. Du, A. Kolchin and H.-P. Cheng, *J. Chem. Phys.*, 2004, **120**, 1044–1054.

- 61 N. Kumar, P. R. C. Kent, A. V. Bandura, J. D. Kubicki, D. J. Wesolowski, D. R. Cole and J. O. Sofo, *J. Chem. Phys.*, 2011, **134**.
- 62 M.-P. Gaigeot, M. Sprik and M. Sulpizi, *J. Phys.: Condens. Matter*, 2012, **24**, 124106.
- 63 G. Tocci and A. Michaelides, *J. Phys. Chem. Lett.*, 2014, **5**, 474–480.
- 64 R. Osuga, T. Yokoi, K. Doitomi, H. Hirao and J. N. Kondo, *J. Phys. Chem. C*, 2017, **121**, 25411–25420.
- 65 L. R. Merte, G. Peng, R. Bechstein, F. Rieboldt, C. A. Farberow, L. C. Grabow, W. Kudernatsch, S. Wendt, E. Lægsgaard, M. Mavrikakis and F. Besenbacher, *Science*, 2012, **336**, 889–893.
- 66 K. L. Geisinger, G. V. Gibbs and A. Navrotsky, *Phys. Chem. Miner.*, 1985, **11**, 266–283.
- 67 K. Vanheusden, P. P. Korambath, H. A. Kurtz, S. P. Karna, D. M. Fleetwood, W. M. Shedd and R. D. Pugh, *IEEE Trans. Nucl. Sci.*, 1999, **46**, 1562–1567.
- 68 B. C. Wood, E. Schwegler, W. I. Choi and T. Ogitsu, *J. Am. Chem. Soc.*, 2013, **135**, 15774–15783.
- 69 T. Takei and M. Chikazawa, *J. Colloid Interface Sci.*, 1998, **208**, 570–574.
- 70 M. Kagan, G. K. Lockwood and S. H. Garofalini, *Phys. Chem. Chem. Phys.*, 2014, **16**, 9294–9301.
- 71 M. B. Webb, S. H. Garofalini and G. W. Scherer, *J. Phys. Chem. C*, 2011, **115**, 19724–19732.
- 72 M. B. Webb, S. H. Garofalini and G. W. Scherer, *J. Phys. Chem. B*, 2009, **113**, 9886–9893.
- 73 T. S. Mahadevan and S. H. Garofalini, *J. Phys. Chem. B*, 2007, **111**, 8919–8927.
- 74 A. K. Soper, *Chem. Phys.*, 2000, **258**, 121–137.
- 75 B. F. Feuston and S. H. Garofalini, *J. Chem. Phys.*, 1989, **91**, 564–569.
- 76 R. H. Henchman and S. J. Irudayam, *J. Phys. Chem. B*, 2010, **114**, 16792–16810.
- 77 H. Haghighi, J. Higham and R. H. Henchman, *J. Phys. Chem. B*, 2016, **120**, 8566–8570.
- 78 S. J. Irudayam and R. H. Henchman, *Mol. Phys.*, 2011, **109**, 37–48.
- 79 R. H. Henchman and S. J. Cockram, *Faraday Discuss.*, 2013, **167**, 529–550.
- 80 R. H. Henchman, *J. Phys.: Condens. Matter*, 2016, **28**.
- 81 H. C. Andersen, *J. Comput. Phys.*, 1983, **52**, 24–34.
- 82 S. H. Lee and P. J. Rossky, *J. Chem. Phys.*, 1994, **100**, 3334–3345.
- 83 P. Gallo, M. Rovere and E. Spohr, *J. Chem. Phys.*, 2000, **113**, 11324–11335.
- 84 P. Gallo, M. A. Ricci and M. Rovere, *J. Chem. Phys.*, 2002, **116**, 342–346.
- 85 N. Giovambattista, P. J. Rossky and P. G. Debenedetti, *Phys. Rev. E: Stat., Nonlinear, Soft Matter Phys.*, 2006, **73**, 041604.
- 86 S. R.-V. Castrillon, N. Giovambattista, I. A. Aksay and P. G. Debenedetti, *J. Phys. Chem. C*, 2011, **115**, 4624–4635.
- 87 T. Takei and M. Chikazawa, *J. Colloid Interface Sci.*, 1998, **208**, 570–574.
- 88 M. E. Tuckerman, D. Marx, M. L. Klein and M. Parrinello, *Science*, 1997, **275**, 817–820.
- 89 M. D. Fayer, *Acc. Chem. Res.*, 2011, **45**, 3–14.
- 90 D. Laage and J. T. Hynes, *Science*, 2006, **311**, 832–835.
- 91 D. Laage and J. T. Hynes, *J. Phys. Chem. B*, 2008, **112**, 14230–14242.
- 92 S. Urashima, A. Myalitsin, S. Nihonyanagi and T. Tahara, *J. Phys. Chem. Lett.*, 2018, **9**, 4109–4144.
- 93 C. Totland, S. Steinkopf, A. M. Blokhus and W. Nerdal, *Langmuir*, 2011, **27**, 4690–4699.
- 94 M. Nogami, *J. Sol-Gel Sci. Technol.*, 2004, **31**, 359–364.